Pullin, H., Springell, R., Parry, S., & Scott, T. (2017). The effect of aqueous corrosion on the structure and reactivity of zero-valent iron nanoparticles. Chemical Engineering Journal, 308, 568-577. DOI: 10.1016/j.cej.2016.09.088

Chemical Engineering Journal 308 (2017) 568–577

Contents lists available at ScienceDirect

Chemical Engineering Journal

journal homepage: www.elsevier.com/locate/cej

The effect of aqueous corrosion on the structure and reactivity of zero-valent iron nanoparticles

Huw Pullin [a,*], Ross Springell [a], Stephen Parry [b], Thomas Scott [a]

[a] Interface Analysis Centre, School of Physics, HH Wills Physics Laboratory, University of Bristol, Tyndall Avenue, Bristol BS8 1TL, United Kingdom
[b] Diamond Light Source, Diamond House, Harwell Science and Innovation Campus, Fermi Avenue, Didcot OX11 0QX, United Kingdom

HIGHLIGHTS

- nZVI retain a Fe^0 core for over 4 w when aged in pure water.
- Goethite is proposed to be the final aqueous corrosion product of nZVI.
- Aqueous corrosion of nZVI has a significant negative impact on remediation reactions.
- Loss of the Fe^0 core led to metal remobilisation from nZVI surfaces.

ARTICLE INFO

Article history:
Received 24 May 2016
Received in revised form 18 August 2016
Accepted 16 September 2016
Available online 17 September 2016

Keywords:
Iron nanoparticles
Ageing
Groundwater
Remediation
Heavy metals
Contamination

ABSTRACT

The following work investigates the effect of aqueous corrosion on the structure of zero-valent iron nanoparticles (hereafter nZVI), and their effectiveness in removing heavy metal contaminants from solution. Our results indicate the corrosion of nZVI is characterised by three periods of activity: i) (<1 d) a rapid change, with the formation of large volumes of amorphous corrosion products (Fe^{3+} hydroxides with considerable adsorbed water, tentatively, ferrihydrite) with concurrent formation of magnetite; ii) (<4 w) the formation of maghemite, a reduction in surface area and a slow transformation to metastable lepidocrocite; iii) (>4 w) a stabilisation of surface stoichiometry and surface area, the loss of all zero-valent iron and the formation of goethite, which is ascribed as the likely final state of nZVI in geochemically simple solutions. This final transformation was continuing as the experiment concluded. All nZVI corrosion products identified in this study have also been identified as existing in natural environments at the same scale lengths. The reactivity of nZVI exhibited a significant reduction with increasing oxidation, although the reduction in reactivity varies according to the contaminant uptake mechanism. From this work, it is proposed that nZVI will have a considerably greater reactive longevity in the natural environment than previously thought, in the order of weeks or months rather than days as previously reported.

1. Introduction

1.1. Iron in the environment

Zero-valent iron nanoparticles are an emerging technology for the treatment of contaminated groundwater. The bulk form of zero-valent iron has been employed for remediation purpose for over twenty years [1], in the form of permeable reactive barriers with reactive materials such as cast iron, steel wool, and amorphous ferric oxide [2]. The corrosion products of these 'filler' materials are fundamentally bulk, static iron oxides, and are ubiquitous in nature (the term iron oxides here refers to both iron oxides, such as wüstite – FeO and iron oxide hydroxides, such as goethite – γ-FeOOH). Despite the ubiquity of these iron phases, concerns have been raised as to the corrosion products of nZVI [3,4], as to whether they are similar to their bulk counterparts.

1.2. The effect of ageing on the structure of nZVI

Due to its high surface area and greater availability of surface reactive sites, nZVI will corrode faster than bulk-Fe^0 [5], but Fe^0 in any form will already have a film of surface oxide acquired directly after synthesis [6–8], typically 3 nm thick [9], but the exact

* Corresponding author.
E-mail address: phxhp@bristol.ac.uk (H. Pullin).

http://dx.doi.org/10.1016/j.cej.2016.09.088
1385-8947/

structure depends on the synthesis process, particle size, and storage conditions [10,11]. On aqueous exposure, it has been suggested that at the shell-water interface, water will disrupt the oxide shell by hydration or autoreduction [12,13], yielding Fe^{2+} species, the stability of which is mostly dependent on local geochemical conditions [14,15]. For waters encountered in nature, Fe^{2+} species are of limited stability and are very sensitive to rapid oxidation by dissolved oxygen (DO) [12], yielding a large array of porous and highly adsorptive iron hydroxides (e.g., $Fe(OH)_2$, $Fe(OH)_3$, ferrihydrites) [16]. The resulting Fe^{3+} species readily hydrolyse, precipitate and transform to various less porous and less adsorptive oxides in the following way: $[Fe(H_2O)_6]^{3+}_{(aq)} \rightarrow Fe(OH)_{3(aq)} \rightarrow Fe(OH)_{3(s)} \rightarrow$ oxides [17], which includes wüstite, magnetite (Fe_3O_4), maghemite (γ-Fe_2O_3) and FeOOH species [16].

Academic studies have recorded numerous iron oxidation products. In chemically simple solutions (i.e. those without a high anionic load), at the end of experimental studies, nZVI have been determined to have transformed to lepidocrocite (γ-FeOOH) [12,18,19], goethite [20–23], magnetite [19,21,23] and maghemite [19,22,24].

1.3. The effect of ageing on the reactivity of nZVI

A small number of studies have examined the effect of corrosion on the reactivity of nZVI. These are summarised in Table 1. However, it has been reported that reactivity (degradation of C_2HCl_3) Another study reported that air-exposure did not significantly effect nZVI reactivity (degradation of C_2HCl_3), although all Fe^0 had been consumed within 11 d [25], although this has been contradicted by other works [11,22].

From the above, it can be stated that there has been limited work concerning the progressive environmental oxidation of nZVI, an idea highlighted in a recent review paper [27], which noted that although ageing has been identified as a significant issue impacting the reactivity of nZVI, limited work has been completed. Therefore, the specific objectives of this study are to map the structural and surface changes to nZVI as it corrodes in a simple solution, and then expand this to investigate how aqueous corrosion effects nZVI reactivity in relation to the uptake to three metal contaminants. The overall aim is to provide underpinning evidence and demonstration that the corrosion products of zero-valent iron nanoparticles are similar to the corrosion products of bulk zero-valent iron, and in this way, allay some of the concerns raised [3,4] as to the use of zero-valent iron nanoparticles for the remediation of contaminated groundwater.

Table 1
Summary of published data on the effect of corrosion on the reactivity of nZVI.

Nanoparticle type	Contaminant	Conclusion
nZVI[H,*]	Carbon tetrachloride (CCl_4)	A decrease in reactivity and Fe^0 content for nZVI exposed to deionised, deoxygenated water for periods up to 6 months [13]
nZVI[H,*]	Carbon tetrachloride (CCl_4)	A decrease in reactivity for nZVI exposed to air for 1 day [22]
nZVI[H,*]	Trichloroethylene (C_2HCl_3)	No decrease in reactivity for nZVI removed from an alkaline slurry for periods up to 2 years [8]
nZVI[B,†]	Trichloroethylene (C_2HCl_3)	No decrease in reactivity for nZVI exposed to air for 3 days [26]
nZVI[B,†]	Bromate ($KBrO_3$)	A decrease in the reactivity for nZVI stabilized with inert gas and then exposed to air and humid air up to 1 month [11]

[*] nZVI manufactured via the high temperature hydrogen-reduction of nanoscale hematite.
[†] nZVI manufactured via the borohydride-reduction of aqueous iron.

2. Materials and methods

2.1. Chemicals

All chemicals (iron sulphate ($FeSO_4{\cdot}7H_2O$), nitric acid (HNO_3), sodium borohydride ($NaBH_4$), sodium hydroxide (NaOH), copper nitrate ($CuNO_3{\cdot}3H_2O$), zinc nitrate ($Zn(NO_3)_2{\cdot}6H_2O$), sodium chromate (Na_2CrO_4) and solvents (ethanol, acetone)) used in this study were of analytical grade. All water used in this study was Milli-Q (resistivity 18.2 MΩ) water.

2.2. Synthesis of nanoparticles

Zero-valent iron nanoparticles were synthesised using borohydride to reduce ferric to a metallic state [28,29]. Briefly, 30.6 g of $Fe(SO_4){\cdot}6H_2O$ was dissolved in 200 mL of water that had been purged with oxygen free nitrogen gas for 10 min. By slowly adding 4 M NaOH dropwise to prevent the formation of hydroxocarbonyl complexes, the solution pH was adjusted to 6.8. To this, 12.0 g of $NaBH_4$ was added (~0.2 g per min), to reduce the Fe^{2+} to Fe^0. The resultant solid material was washed through centrifugation and sequential rinsing in 50 mL of water, acetone and then ethanol. The nanoparticles were dried under low vacuum in a vacuum desiccator (~10^{-2} mbar), and then stored in an argon filled (BOC, 99.998%) MBraun glovebox to prevent further oxidation until required.

2.3. Effect of aqueous corrosion on structure and surface chemistry

To assess bulk and crystallinity changes to nZVI, a 5 L aspirator bottle was filled with 5 L of water and 5.0 g of nZVI (leaving ~100 mL headspace). The nZVI were dispersed by agitating the aspirator bottle for 5 min. From this, aliquots of 500 mL of nZVI-liquid were removed periodically after agitation: 2 h, 1 d, 3 d, 1 w, 2 w, 4 w, 8 w, and 16 w. These aliquots were centrifuged at 5000 rpm for 10 min using an Eppendorf 5810 bench-top centrifuge, and then the supernatant decanted. The remaining solid material was cleaned using the same sequential washing method used in Section 2.2. The oxidised nZVI were stored under clean ultra-pure ethanol before analysis (typically 24 h). The nZVI for BET analysis were dried and stored using the same method used in Section 2.2. Headspace was not controlled within the aspirator bottle during the experiment and so comprised of ambient air.

2.4. Effect of aqueous corrosion on reactivity

The effect of aqueous corrosion on the reactivity of nZVI was assessed using three metal contaminants, divalent copper (Cu) and zinc (Zn) and hexavalent chromium (Cr(VI)) chosen for their differing uptake inter-reactions with zero-valent iron nanoparticles (reduction, adsorption and reduction-precipitation respectively). [30] For each metal contaminant, eight 250 mL Pyrex beakers were filled with 190 mL of pH 4 (adjusted using 0.1 M HCl) Milli-Q water. To each, except one blank (nZVI free) solution, 0.5 g L^{-1} of nZVI were added. All batches were sonicated in a VWR USC100T ultrasonic bath for 5 min after nZVI addition to aid dispersion, and then covered loosely with thin, clear, laboratory plastic film to allow gas exchange but to prevent evaporation and cross contamination.

After the required ageing period: unaged, 2 h, 1 d, 3 d, 1 w, 2 w and 4 w (the last time point which Fe^0 was detected), an aqueous

metal contaminant that had been adjusted to pH 4 using either 0.1 M HNO_3 or 0.1 M NaOH was added to each batch. For divalent Cu(II) and Zn(II), initial concentrations were 50 mg L^{-1}, while Cr (VI) was 20 mg L^{-1}.

Each batch system was sampled at 0, 1, 2.5, 5, 10, 20, 40, 80, 160, 320 and 640 min, as well as 1 d, 3 d, and 7 d. At the same time point, geochemical parameters (pH, Eh and DO) were measured with a Hach HQ40d Multimeter. To ensure sample homogeneity, the beakers were gently agitated prior to sampling and geochemical measurement. A solid sample for analysis was retained at the completion of the experiment for further analyses. From each beaker, 10 mL aliquots were withdrawn, and the solid and liquid phases were separated by centrifugation at 6500 rpm for 1 min in a Hamilton Bell Vanguard V6500 desktop centrifuge. The resultant liquid was syringe-push filtered (0.22 μm cellulose filter), and then acidified using 1% v/v concentrated nitric acid to prevent metal precipitation or adsorption to the sample vessel. The remaining solid material was cleaned using the same sequential washing method as outlined in Section 2.2. The samples were stored under ultra-pure ethanol until analysis (<24 h).

2.5. Sample analysis methods

Specific surface area (SSA) was determined by Brunauer-Emmett-Teller (BET) analysis using a Quantachrome NOVA 1200 instrument. A known weight of the dried, vacuum degassed ($\sim 10^{-2}$ mbar for 12 h at 75 °C) material was analysed using nitrogen as the adsorbent and following a 7 point BET method. Transmission electron microscopy (TEM) images of nZVI mounted on 200 mesh holey carbon coated copper grids were obtained with a JEOL JEM 1200 EX Mk 2 TEM, operating at 120 keV. A Phillips Xpert Pro diffractometer with a Cu radiation source (CuK_α 1.5406 A°) was used for X-ray diffraction (XRD) analysis (generator voltage of 40 keV; tube current of 30 mA), and plots were acquired between 10 and 70° 2θ, with a step size of 0.02° and a 2 s dwell time. A Thermo Scientific K-Alpha$^+$ spectrometer employing a monochromatic source (AlK_α 1486.6 eV) was used for X-ray photoelectron spectroscopy (XPS) analysis. Data analysis was performed using the CasaXPS package [31]. Fe $2p_{3/2}$ peak was fitted according to the method of Grosvenor et al., (2004) [32], and the O 1 s peak according to the method of Li and Zhang (2004) and Abdel-Samad and Watson (1997). [30,33] X-ray absorption spectroscopy (XAS) spectra were collected at Beamline B18 at the Diamond Light Source, Harwell, UK from pelletised samples in transmission mode at room temperature. The storage ring was operating in a 10 min top-up mode for a ring current of 250 mA and an energy of 3 GeV. The radiation was monochromated with a Si(1 1 1) double crystal, and harmonic rejection was achieved through the use of two platinum-coated mirrors operating at an incidence angle of 8.0 mrad. The monochromator was calibrated using the K-edge of an iron foil, taking the first inflection point in the Fe-edge as 7112 eV. Samples for XAS were prepared in an MBraun argon filled glove box by grinding 3 mg of nZVI with 50 mg of cellulose in an agate mortar for 3 min. The subsequent homogenous mixture was pressed into an 8 mm pellet and then sealed with Kapton tape. Obtained spectra were summed and background-subtracted using the software package Athena. (Demeter 0.9.24; Ravel and Newville, 2005). Sample composition was then determined using the linear combination fitting (LCF) routine of Athena. The X-ray absorption near edge structure (XANES) spectra were fitted against spectra of known standards using a fitting window of −20 to +53 eV from 7112 eV [34]. Inductively-coupled plasma optical emission spectroscopy (ICP-OES) was used to analyse aqueous metal concentrations, the instrument employed being an Agilent 710.

3. Results and discussion

3.1. Changes to structure due to aqueous corrosion

The changes to nZVI crystallinity (XRD scans) and size (TEM images) due to aqueous oxidation are recorded in Figs. 1 and 2 respectively, while XANES spectra are shown in Fig. 3. Surface area as determined by BET, and results from XPS fitting of the Fe $2p_{3/2}$ and O 1s peaks are presented in Table 2. The identified iron forms as identified by XRD and XANES analysis are also presented. Due to the limited extent of the oxide layer in nZVI and the similar spinel crystal structure of both maghemite and magnetite, their differentiation by XRD is extremely difficult [24,35]. These phases were differentiated using XANES analysis.

3.1.1. As-formed nZVI

Characterisation of the as-formed nZVI revealed typical features associated with other studies using borohydride-reduced zero-valent iron nanoparticles [29]. Analysis by XRD (Fig. 1), XAS (Fig. 3) and XPS (Figs. S1 and S2 – Supporting information) indicated that the core of nZVI was poorly crystalline α-Fe (characteristic XRD peak at 44.9 °2θ) with a shell of mixed valent iron oxides/oxyhydroxides. Fitting of the XANES data (Fig. 3) indicated the presence of Fe^0, along with 2-line ferrihydrite, (tentatively given as $Fe_5O_8H{\cdot}H_2O$) [36], although near 20% of the total fit was undetermined. The presence of 2-line ferrihydrite is discussed in more detail below, although the presence of this iron form does suggest that the surface of the unaged nZVI contained little crystalline iron oxide phases that have previously been reported, such as wüstite [37], magnetite [38], maghemite or FeOOH [30,39]. Siskova et al. (2012) stated that the shell of borohydride-reduced particles were Fe^{3+} oxide/hydroxide of an unspecified ratio [40], which is in broad agreement with the results in this work. The as-formed shell composed of a number of mixed-valent iron oxide hydroxides, with hydroxide being the more prevalent form (XPS determined stoichiometric ratio of the O 1 s peak of OH^-:O^{2-} of 5). TEM analysis determined that the particles were roughly spherical (Fig. 2, Panel 'unaged'), with an approximate range of 40–100 nm, and an observable dark core surrounded by a lighter oxide layer, although no clear grain structure was identifiable. BET analysis determined that the surface area of nZVI was 11.5 m^2 g^{-1}.

3.1.2. Up to 1 d aqueous exposure

After 1 d of exposure, the surface area of the corroding nZVI increased over tenfold, to 160.8 m^2 g^{-1}. This change was attributable to the formation of a large volume of corrosion products, and/or cracking and pitting of the shell due to corrosion propagated strain; both processes have been previously observed [41,42]. The corrosion products can be observed as 'lacy' areas on the surface of the nanoparticles (Fig. 2, Panel *2h* and *1d*), although the core of the particles remains dark, indicative of zero-valent iron, confirmed by the XRD analysis. It is not possible to determine whether these lacy products are from dissolution and precipitation, or from surface reactions [42]. However, the broad arc around 25 °2θ in the 2 h XRD plot has been assigned as ferrihydrite in other corrosion studies [43,44], which would form at the surface of corroding nZVI. Linear combination fitting of the XANES 2 h data does indicate the presence of 2-line ferrihydrite, although this nZVI sample appears more oxidised than the 1 d or 3 d spectra; this could be due to the presence of greater amounts of heterogeneous amorphous metastable oxidised iron species than at later time points, or possibly oxidation during analysis. This fits well with the observed increase in SSA, as ferrihydrite has a reported volume 6.4 times larger than the equivalent mass of nZVI [42]. Ferrihydrite has various reported formulas, including $Fe_5HO_8{\cdot}H_2O$ [36] and $FeOH_3{\cdot}3H_2O$ [42] and so

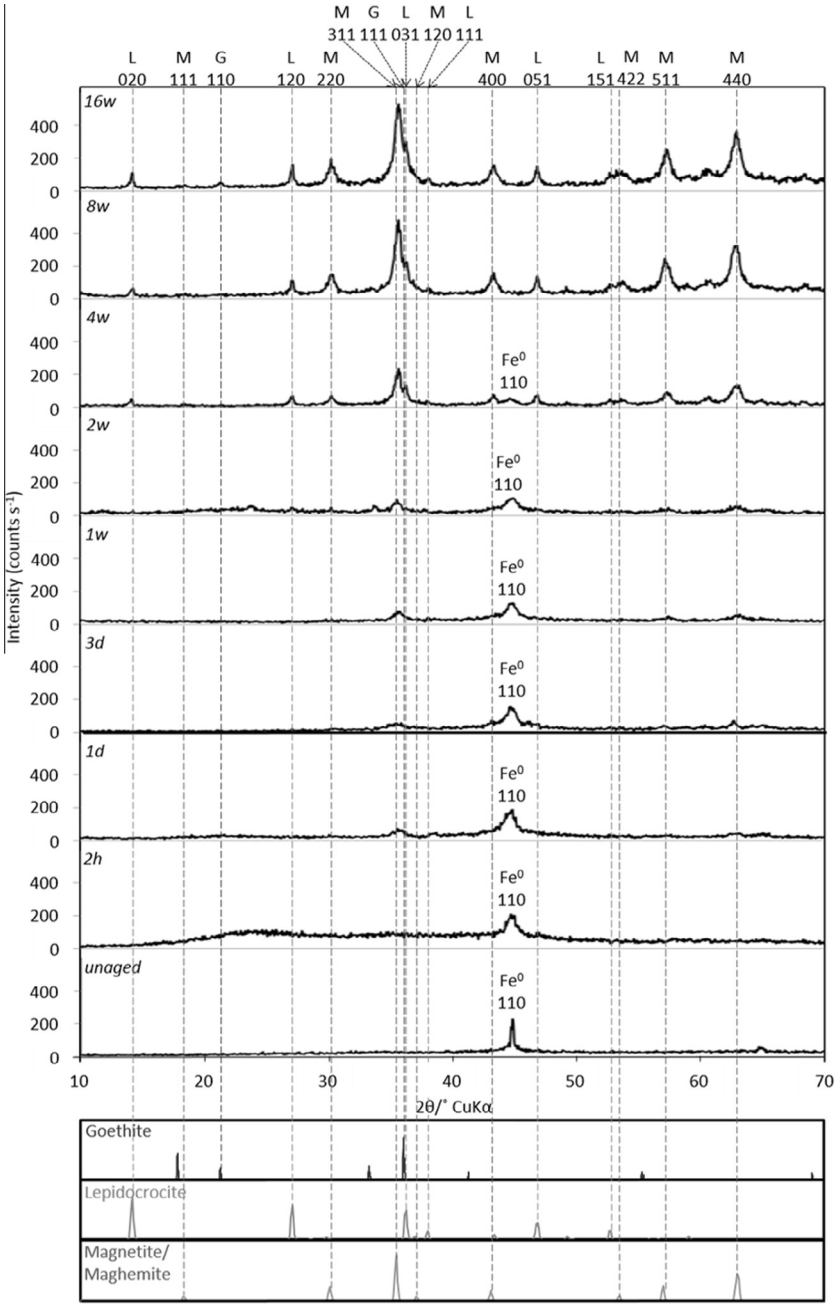

Fig. 1. X-ray diffraction plots with assigned Miller Indices (for the range 10–70 °2θ) acquired for unaged, 2 h, 1 d, 3 d, 1 w, 2 w, 4 w, 8 w and 16 w nZVI (ascending). Key: G – goethite, L – lepidocrocite and M – magnetite/maghemite.

the XPS determined surface stoichiometry in this study agrees well with the latter. Ferrihydrite will not develop greater crystallinity over time, but transforms to other iron hydroxides with associated dehydration [36]. The emergent XRD peaks at 35.6 and 57.6 °2θ were assigned to magnetite/maghemite, the first phase detected other than Fe^0. Both these iron oxides contain octahedral and tetrahedral iron [45,46]. At the shell, the lack of Fe^{2+} probably excludes the presence of magnetite [36], and therefore it is proposed that magnetite transforms, at least in part, to maghemite. This agrees with a study by Nagayama and Cohen [47], which concluded that the oxide layer on iron consists of an inner layer of magnetite and an outer layer of maghemite. However, as stated, in this work ferrihydrite was also identified.

3.1.3. Up to 4 w aqueous exposure

Linear combination fitting of the XANES analysis of nZVI aged between 3 d and 4 w indicated the formation of magnetite (24.1%) after 1 w, and reduction in the proportion of maghemite to 45.6%. After 2 w exposure, LCF indicated the sample was composed of magnetite (61.3%), maghemite (27.2%) and lepidocrocite (4.3%). After 4 w, XANES LCF analysis showed maghemite and lepidocrocite dominate (33 and 53.6% respectively), with no magnetite identified. Various surface and bulk parameters indicated a slowing of the transformation processes (Fig. 4). An increase in XPS determined $Fe^{3+}_{octrahedral}$:$Fe^{3+}_{tetrahedral}$ ratio suggests the formation of more thermodynamically stable Fe^{3+} compounds [48]. Images obtained from TEM indicated the reduction in the particle size and

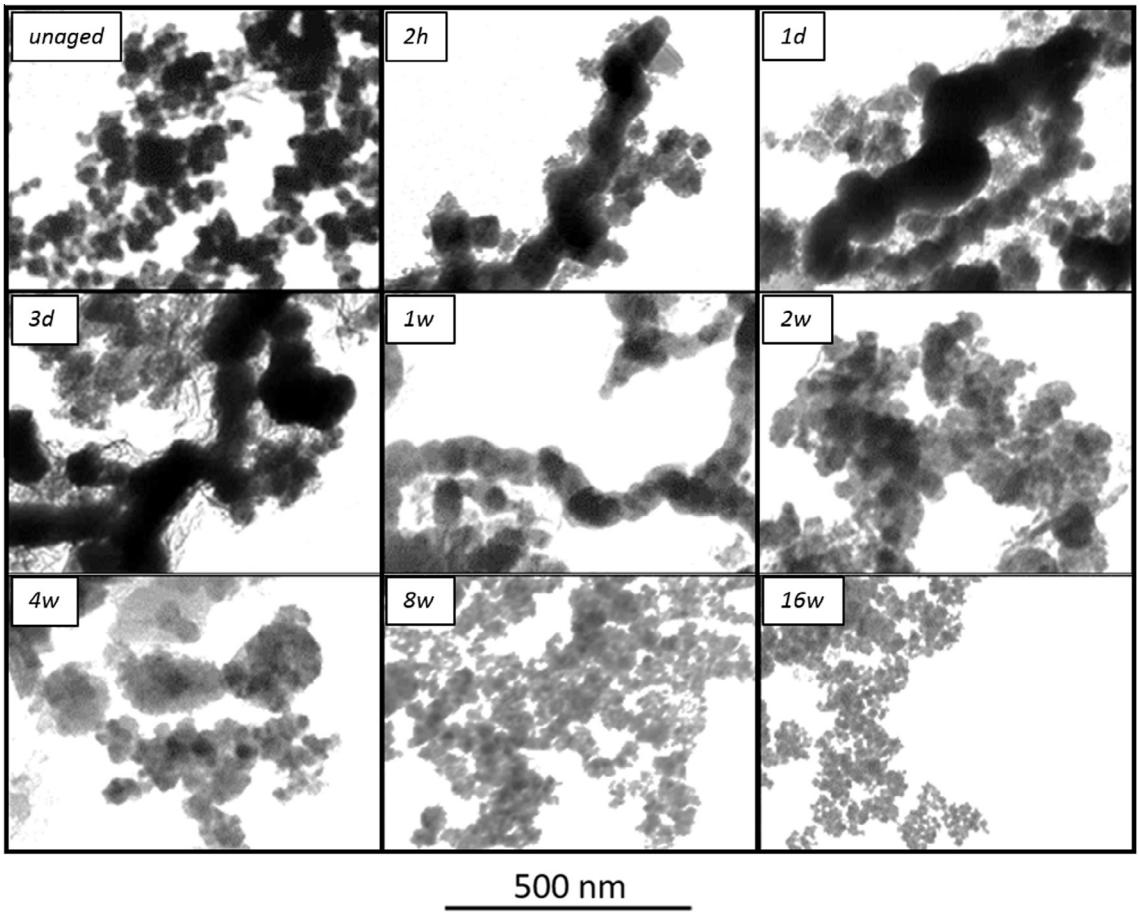

Fig. 2. TEM images acquired for unaged, 2 h, 1 d, 3 d, 1 w, 2 w, 4 w, 8 w and 16 w nZVI.

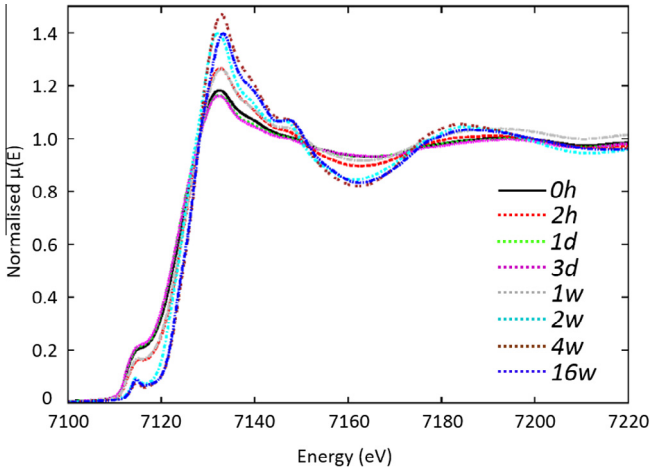

Fig. 3. XANES spectra obtained for unaged, 2 h, 1 d, 3 d, 1 w, 2 w, 4 w and 16 w nZVI.

the amounts of 'lacy' corrosion products (Fig. 2, Panel *1w*). A lightening of the nanoparticle core colour, with larger areas of grey oxides/hydroxides, inferred the expenditure of the Fe^0 fraction of the particle. At 4 w, XRD plot and XAS LCF analysis clearly demonstrated the mixed iron nature of the particles with zero-valent iron (44.9 °2θ), magnetite/maghemite (30.2, 35.6 and 57.6 °2θ) and lepidocrocite (14.1, 27.1, 36.3 and 38.1 °2θ) all identified. This latter phase has been observed as a corrosion product in previous studies [12,18,36]. After this time point, the zero-valent peak at 44.9 °2θ was either absent or too small in intensity to be detectable. This is in agreement with the XAS LCF analysis.

3.1.4. Post 4 w aqueous exposure

This period of nZVI corrosion could be described as a slow transformation of the iron oxide and oxyhydroxide phases, rather than the more rapid changes identified at shorter timescales. Maghemite (as identified by XANES analysis, Fig. 3 and Table 2) and lepidocrocite were detected in the 8 w XRD scan, but at 16 w, goethite was also identified (21.3 °2θ). Goethite could be included in the fit of the XANES signal (at ~3%), although the fit was not significantly improved by its inclusion. Goethite is, along with hematite, the most thermodynamically stable iron compound and therefore the end member of many transformation routes [36]. Analysis by XPS indicated that (physically and/or chemically) adsorbed surface water had reduced from 13.7% of the O signal at 4 w to 1.3% by 16 w. All fine grained iron materials contain up to several percent of adsorbed water [15], and so this value could be indicative of a final, stable state. At 4 w, the OH^-:O^{2-} ratio of the nanoparticle surface was 0.8, and $Fe^{3+}_{octahedral}$:$Fe^{3+}_{tetrahedral}$ ratio was 2.6; by 16 w, these values were 0.9 and 2.3 respectively. The 16 w O^{2-}:OH^- ratio agreed well with reported values for iron oxyhydroxide phases such as lepidocrocite (0.9–1.1). [33,49] However, the continued presence of tetrahedral Fe^{3+} indicated that the shell chemistry is not homogeneous; the latter phases of iron oxidation, such as lepidocrocite, goethite and hematite do not contain Fe^{3+} in tetrahedral coordination [45]. The 8 w, and to a greater extent the 16 w, XRD scans indicated greater crystallisation than the 4 w nanoparticles, with more defined peaks detected for each phase, and a continued reduction

Table 2
Identified iron forms, SSA values and XPS fitting of the Fe $2p_{3/2}$ and O 1s spectra.

Age	Identified Fe forms*	SSA ($m^2\ g^{-1}$)	Iron Fitting (%)†				Oxygen Fitting (%)‡		
			Fe^0	Fe^{2+}_{Oct}	Fe^{3+}_{Oct}	Fe^{3+}_{Tet}	O^{2-}	OH^-	H_2O
Unaged	Fe^0, F	11.5	8.06	12.1	71.7	8.2	11.3	60.5	28.2
2 h	Fe^0, F	112.5	0.61	2.8	46.1	50.5	11.4	44.4	44.2
1 d	Fe^0, F, Mn	160.8	0	0	44.7	55.4	9.1	29.5	61.4
3 d	Fe^0, F, Mn	136.1	0	0	56.3	43.5	14.8	40.8	44.4
1 w	Fe^0, F, Mn	95.1	0	0.3	56.5	43.3	21.5	50.4	28.1
2 w	Fe^0, F, L, Mn, Mh	91.5	0	0	58.8	41.2	21.7	41.4	36.9
4 w	Fe^0, F, Mh	65.8	0	0	70.1	29.9	48.8	37.5	13.7
8 w	L, F, Mh§	57.4	0	0	70.2	29.8	49.8	43.2	7.0
16 w	L, F, Mh, G	57.8	0	0	72.9	27.1	52.8	45.9	1.3

Key: Fe^0 – zero-valent iron, F – ferrihydrite, G – goethite, L – lepidocrocite, Mh – maghemite and Mn – magnetite.
* Identified through XRD plots and LCF of XANES data (Figs. 1 and 3).
† Identified through fitting of the Fe $2p_{3/2}$ XPS spectra (Figs. S1 and S2 – Supporting information).
‡ Identified through fitting of the O 1s XPS spectra (Figs. S1 and S2 – Supporting information).
§ Due to limited experimental time, XANES analysis was not performed on nZVI aged for 8 w. This information is from XRD only.

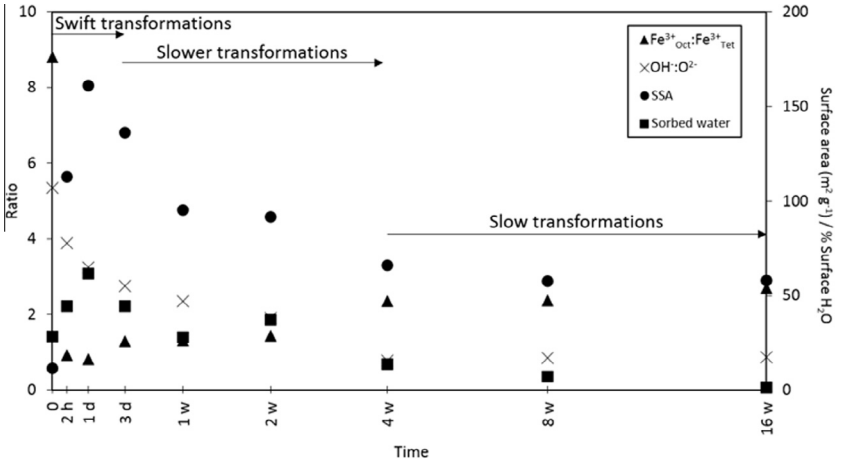

Fig. 4. Time resolved SSA and XPS determined surface changes to corroding nZVI. Key: Triangle – Ratio of surface $Fe^{3+}_{octahedral}$:$Fe^{3+}_{tetrahedral}$, Cross – Ratio of surface OH^-:O^{2-} (both left hand scale), Circle – SSA and Square – % of adsorbed surface water (both right hand scale).

in the size of the predominantly grey particles (42 nm at 8 w, 36 nm at 16 w). Specific surface area had stabilised after 8 w at ~57 $m^2\ g^{-1}$. Reported surface areas of nanoparticulate iron corrosion products include goethite, ~25 $m^2\ g^{-1}$ [15], lepidocrocite, ~68 $m^2\ g^{-1}$ [50]. maghemite, ~40 $m^2\ g^{-1}$ [51], and magnetite, ~50 $m^2\ g^{-1}$ [7]. These figures indicate that the 16 w nanoparticles are a mixed-phase iron corrosion product. Of note, LCF of the XANES signal indicate the presence of 2-line ferrihydrite in all aged nZVI, indicating that transformation processes were continuing up to the termination of the experiment.

3.1.5. Summary of pathway of nZVI aqueous corrosion

With respect to the above, the first step in the transformation of nZVI is the conversion of zero-valent (or ferrous iron) by oxidation with DO or water to form magnetite. Magnetite can be further oxidised to maghemite [36]. Lepidocrocite is formed through the oxidation of dissolved ferrous ions or magnetite/maghemite. Finally, lepidocrocite oxidises to the thermodynamically more stable goethite [36,52]. This reaction series can be inferred from the recovery and analysis of hydrogen-reduced iron nanomaterial from a field pilot study [53]. After near four months aqueous oxidation of nZVI, the resultant material was identified as mixed phase magnetite/maghemite, lepidocrocite, goethite nanoparticles. The emergence of this latter phase revealed that corrosive transformation had not reached an endpoint.

3.2. Changes to nZVI reactivity due to aqueous corrosion

3.2.1. Starting solution geochemistry

For batches treated with unaged (i.e. as-formed) nZVI, with the addition of the contaminant and nZVI, a rapid shift to chemically reducing, anaerobic, raised pH (~8) conditions was observed, with Eh minima recorded in all systems within 120 min (Fig. S3 – Supporting information). All 2 h, 1 d and 3 d solutions were experiencing negative redox, raised pH and low DO (<2.0 mg L^{-1}) conditions at the commencement of the experiment, indicating that nZVI corrosion was well advanced. This is in contrast to both the 1 w, 2 w and 4 w solutions, where starting Eh, pH and DO conditions were similar to the control. Starting iron concentrations are shown in Table 3.

3.2.2. Changes to solution metal concentration

The maximum uptake and final retention of metals by nZVI aged for differing times, as well as rate constants, are shown in Table 4 and Fig. S4 – Supporting information. A comparison of reaction kinetics is shown in Fig. 5. From these, it is evident that irrespective of nanoparticle age, a metal uptake response was observed in all solutions. A linear regression of measured data points indicates a pseudo-first-order reaction [20]. The first step in any surface mediated reaction is the adsorption of the reactants onto the adsorbent surface [54], and the subsequent slowing of the

Table 3
Starting iron concentrations (mg L^{-1}) for solutions of nZVI aged for differing times.

Contaminant	Unaged	2 h	1 d	3 d	1 w	2 w	4 w
Cr	0.010	8.499	5.934	2.651	1.332	0.060	0.000
Cu	0.007	8.640	6.591	2.669	1.237	0.052	0.008
Zn	0.008	8.512	6.394	2.527	1.375	0.067	0.004

Table 4
Maximum uptake and retention of metals by nZVI aged for differing times.

Cr(VI) (20 mg L^{-1})	Unaged	2 h	1 d	3 d	1 w	2 w	4 w
Lowest solution concentration (mg L^{-1})	0.16	0.14	0.16	0.17	0.15	0.16	12.9
Final solution concentration (mg L^{-1})	0.16	0.16	0.16	0.17	0.16	0.16	12.9
Rate constant (0–160 min) (k, h^{-1})	0.0048	0.0271	0.0088	0.0054	0.0056	0.0051	0.0032
Cu (50 mg L^{-1})	Unaged	2 h	1 d	3 d	1 w	2 w	4 w
Lowest solution concentration (mg L^{-1})	ND	ND	ND	ND	23.05	26.10	22.64
Final solution concentration (mg L^{-1})	14.04	15.67	24.05	29.36	27.66	28.53	27.92
Rate constant (0–160 min) (k, h^{-1})	N/A	N/A	N/A	N/A	0.0047	0.0031	0.0028
Zn (50 mg L^{-1})	Unaged	2 h	1 d	3 d	1 w	2 w	4 w
Lowest solution concentration (mg L^{-1})	1.64	2.72	7.44	20.61	23.85	32.80	34.75
Final solution concentration (mg L^{-1})	6.59	14.36	22.71	21.67	28.68	32.80	34.75
% Remobilised	86.85	71.33	54.66	56.74	42.76	34.53	30.64
Rate constant (0–160 min) (k, h^{-1})	0.0143	0.0113	0.0081	0.0052	0.0034	0.0009	0.0005

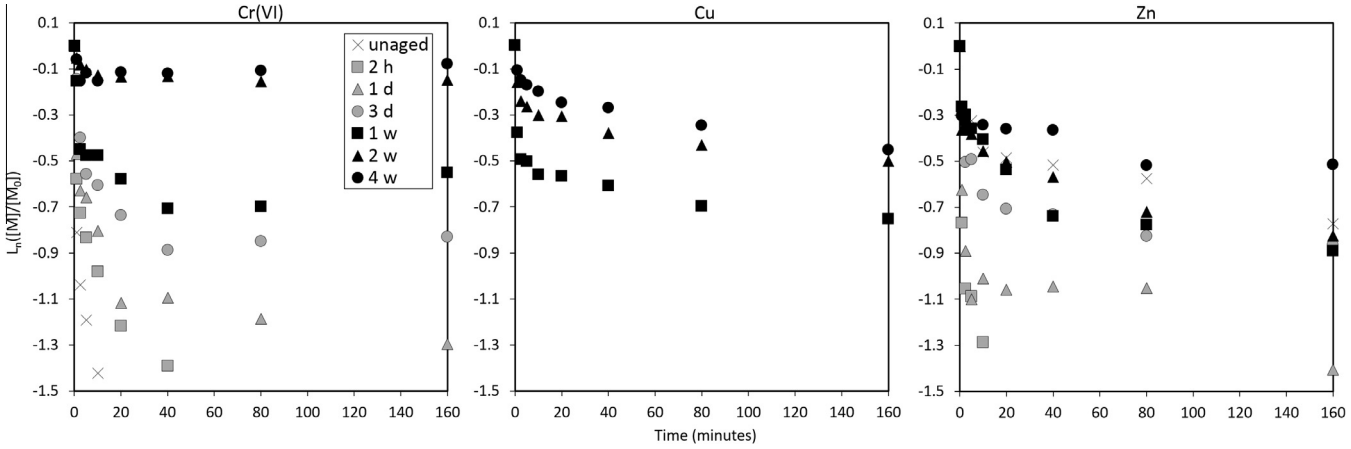

Fig. 5. Comparison of first-order kinetics for the uptake of Cr(VI) (top left), Cu (top right) and Zn (bottom left) from solution when treated with aged nZVI. Key: X – Unaged, Open Square – 2 h, Open Triangle – 1 d, Open Circle – 3 d, Closed Square – 1 w, Closed Triangle – 2 w, Closed Circle – 4 w and Cross – control.

rate has been ascribed to a physical occlusion of the zero-valent iron surface sites, rather than a chemical mechanism [20]. From Fig. 5, this phenomenon can be observed during which the contaminant is removed from solution significantly faster at the commencement of the experiment than at later times. Due to the swift reaction rates, only the most aged nZVI (1 w, 2 w and 4 w) can be plotted for the Cu solution. It can be observed that a different response is elicited by aged nZVI depending on the contaminant treated, although a general decrease in rate constant is commensurate with an increase in the oxidation/age of the nZVI. Furthermore, it can also be seen that for Cu and Zn, final solution concentrations (after 7 d) were generally higher than the lowest concentration recorded, i.e. without external influence, the previously removed metal was released from the nZVI surface. This contaminant remobilisation mechanism is discussed below.

In the Cr(VI) batch systems, only the 4 w nZVI did not exhibit significant removal; no remobilisation was recorded in any of the solutions. In the Cu batch systems,<3 d nZVI completely removed the contaminant from solution, but all nZVI batches experienced contaminant remobilisation after an initial removal spike. Irrespective of age, no nZVI removed the totality of Zn from the solution. In these batches, the contaminant was released from the less corroded nZVI (<1 w), but not from nZVI that had been aged for greater periods.

From the above, it can be stated that the removal efficiency of nZVI is significantly affected by its corrosion state, although the reduction in efficiency is specific to the contaminant uptake mechanism (discussed below). However, a general trend was observed, with decreasing reactivity as nanoparticle age increased. This is attributable to a reduction in electron transfer, due either to a reduction in Fe^0 volume/Fe^{2+} dissolution, or an increase in the surface oxide layer hindering electron transfer.

Chromate removal by nZVI occurs via reduction and precipitation [55], although aqueous Fe rapidly reacts with Cr^{6+} to promote precipitation of insoluble $Cr(OH)_3$, Fe^{3+}-Cr^{3+} hydroxide and/or Fe^{3+}-Cr^{3+} oxyhydroxide [56–59]. In this experiment, it is thought that this second reaction dominated, with calculated rate constants generally decreasing with increasing age, tallying with starting Fe concentration (Table 3). However, the unaged nZVI solution, with no initial aqueous Fe, had the lowest reaction rate of any tested. In this solution, removal would predominantly be via the former

mechanism. This process is accompanied by Cr^{3+} incorporation into the iron oxyhydroxide shell to form mixed Fe and Cr oxyhydroxides [60,61]. This layer acts as an inhibitory layer on the iron surface [58,62], reducing the availability of surface adsorption sites and blocking Fe dissolution, and perhaps also inhibiting the formation of the voluminous corrosion products as observed in the structural experiments (and as such, the unaged nZVI would have the smallest SSA of all particles tested). This inhibition effect was observed in the dampened Cr(VI) solution geochemical response (as compared to the Cu and Zn solutions) on addition of unaged nZVI (Fig. S3 – Supporting information), although XRD scans of all post experimental nanomaterial indicated corrosion reactions had occurred (i.e. no Fe^0 remaining). The 2 h nanoparticles, with the largest surface area, removed chromate at the fastest rate. This, as stated, would be due to the 'primed' aqueous Fe in the solution, but may also be ascribed to the increase in SSA, substantiated by a previous study that found the second recharge of recycled nZVI (with the greatest surface area) reduced nitrate at the fastest rate of the six recharges tested [63].

As stated, for Cu, the initial uptake reaction was so rapid that a rate constant could not be calculated for the nZVI aged <3 d. However, like Cr, rate constants decreased with increasing nZVI age. The Cu uptake mechanism by nZVI has been reported to be surface reduction [30], and therefore a source of electrons must be present, as evidenced in all nZVI batch systems, irrespective of age. Unlike Cr, Cu does not become incorporated into the iron structure, and is susceptible to remobilisation, as evidenced in all nZVI batch systems, irrespective of age. Geochemical data (Figs. S3 and S4 – Supporting information) indicated that Cu remobilisation began after DO entered the system. The availability of oxygen determines the oxidation of Cu in aqueous solutions, with Cu generally assumed to be immune to corrosion by water itself [64]. Therefore, oxygen ingress did not initiate desorption of Cu from the nZVI surface, which suggests that continuing electron transfer is essential for the Cu to remain in a reduced state when DO is present.

The removal mechanism of Zn by nZVI is thought to be by adsorption to the iron hydroxide shell, followed by zinc hydroxide complexation [65], and that this reaction includes electrostatic interactions and specific surface bonding, with no net electron transfer [30]. The reduced contaminant uptake as compared to Cu suggests that this uptake mechanism requires greater, perhaps continued electron flow for Zn to associate with the nZVI surface, and that when electron flow ceases, the cation would be repelled as the Fe surface would be positively charged at the pH values encountered after ~360 min [36,37]. Remobilisation did not occur with the 2 w and 4 w nZVI. It is thought that >2 w, FeOOH is the dominant iron compound at the surface, which has been shown to have a high adsorption affinity for aqueous Zn [65]. This suggests that perhaps two uptake mechanisms are occurring, one propagated by electron flow, and a second (more stable) Zn-FeOOH adsorption reaction.

4. Conclusions

i) Zero-valent iron nanoparticles retain a zero-valent core for over 4 w when aged in pure water;
ii) The corrosion of nZVI is characterised by three periods of activity. Initially, (<1 d) a swift reaction occurs with the formation of large volumes of amorphous corrosion products and the emergence of magnetite. Following this, corrosion slows (<4 w), with the conversion of magnetite to maghemite and the formation of the metastable iron product lepidocrocite. After this period, nZVI corrosion was observed to be very slow, with increasingly small changes and the emergence of goethite, which is likely to be the final state of nZVI in pure solutions;
iii) The aqueous ageing of nZVI has a significant negative impact on the rate constants of metal removal by nZVI, although the reduction in efficiency is specific to the contaminant uptake mechanism. This was attributable to a reduction in electron transfer, due either to a reduction in Fe^0 volume/Fe^{2+} dissolution, or a thickening of the surface oxide/hydroxide layer hindering electron transfer. However, even after 4 w aqueous exposure, nZVI removed 36% Cr^{6+} from a 20 ppm solution, and 55% and 31% of Cu and Zn respectively, from a 50 ppm solution;
iv) Despite impressive initial uptake, both Cu and Zn subsequently remobilised from the surface of nZVI, ascribed foremost to the disappearance of the zero-valent core, and then subsequently by the ingress of DO. Zinc was observed to require greater electron flow to remain associated with the Fe surface than Cu.

5. Context and implications

The current work attempted to assess the longevity and corrosive transformation products of nZVI in the environment when they are utilised for the remediation of contamination. It appears that the 16 w experimental period was not of sufficient duration to assess the problem fully, but certain conclusions may be drawn: the ultimate iron corrosion product we ascribe as goethite, and the transformational process to reach this phase is significant, in the order of months, rather than days. The above suggests that the risk to receptors by nZVI may be a longer-term problem than previously thought. If deployed on site, would require periodic sampling of downstream boreholes to assess the migration of the reactive particles. However, reactivity is a loose term; a stricter definition of reactivity is needed to assess whether only transformation of nZVI to magnetite/maghemite would be considered reactive, or does this term include the further transformation to oxyhydroxides. This, obviously, will determine the regulatory defined length of any sampling regime.

An interesting finding in the current work is the continued reactivity of nZVI, even after 4 w of aqueous ageing. Furthermore, this experiment indicated that, with only a small fraction of the zero-valent core remaining, reductive reactions could still occur. This suggests that deployed nZVI could be suitable for the treatment of a migrating contaminant plume. Due to the significant desorption exhibited in both the Zn and Cu solutions, it is unlikely that nZVI would be employed for the long-term treatment of these contaminants in groundwaters readily supplied with atmospheric oxygen. Chromate, conversely, experienced no desorption, despite a fall in rate constant as the age of the nZVI increased. Therefore, nZVI could prove effective for the treatment of Cr^{6+} plumes at most any subsurface depth for days or weeks after initial dosing, and as reactive rates exhibit a delay before activation, no reductive loss would be experienced if the particles were deployed as a slurry. In fact, a small amount of ageing proved advantageous for the treatment of this contaminant.

It is accepted that the above work has concentrated on geochemically simple waters, and does not take into account the influence of a more complex groundwater on nZVI corrosion. This suggests that a field-scale pilot-study should be undertaken prior to deployment to assess the influence of site geochemistry on the corrosion/reactivity of nZVI.

Acknowledgements

We would like to thank Mr Jonathan Jones (School of Chemistry) from the University of Bristol for performing TEM analysis; Dr Anders Barlow, at the NEXUS facility, Newcastle University for

performing XPS analysis; Dr Chung Choi with help and use of the ICP-OES instrument; and Dr Judith Monnier for providing XANES spectra of standards. We acknowledge Diamond Light Source for time on B18 under proposal SP10173-1.

Appendix A. Supplementary data

Supplementary data associated with this article can be found, in the online version, at http://dx.doi.org/10.1016/j.cej.2016.09.088.

References

[1] S. Warner, B. Longino, M. Zhang, P. Bennet, F. Szerdy, L. Hamilton, in: The first commercial permeable reactive barrier composed of granular iron: Hydraulic and chemical performance at 10 years of operation, in: G.A. Boshoff, B.D. Bone (Eds.), First Int. Symp. Permeable React. Barriers; IAHS Publ. 298, International Association of Hydrological Sciences, Belfast, Northern Ireland, 2005, p. 32, <http://books.google.co.uk/books?id=IZpn94d_3zsC>.
[2] A. Henderson, A. Demond, Long-term performance of zero-valent iron permeable reactive barriers: A critical review, Environ. Eng. Sci. 24 (2007) 401–423.
[3] The Royal Society, The Royal Academy of Engineering, Nanoscience and Nanotechnologies: Opportunities and Uncertainties, The Royal Society and The Royal Academy, 2004.
[4] P. Bardos, B. Bone, D. Elliott, N. Hartog, J. Henstock, P. Nathanail, A risk/benefit approach to the application of iron nanoparticles for the remediation of contaminated sites in the environment, DEFRA, 2011.
[5] C. Macé, S. Desrocher, F. Gheorghiu, A. Kane, M. Pupeza, M. Cernik, P. Kvapil, R. Venkatakrishnan, X. Zhang, Nanotechnology and groundwater remediation: a step forward in technology understanding, Remediat. J. 16 (2006) 23–33.
[6] M. Dickinson, T.B. Scott, R.A. Crane, O. Riba, R.J. Barnes, G.M. Hughes, The effects of vacuum annealing on the structure and surface chemistry of iron: nickel alloy nanoparticles, J. Nanoparticle Res. 12 (2010) 2081–2092.
[7] R. Crane, M. Dickinson, I. Popescu, T. Scott, Magnetite and zero-valent iron nanoparticles for the remediation of uranium contaminated environmental water, Water Res. 45 (2011) 2931–2942.
[8] Y. Liu, G. Lowry, Effect of particle age (Fe^0 content) and solution pH on NZVI reactivity: H_2 evolution and TCE dechlorination, Environ. Sci. Technol. 40 (2006) 6085–6090.
[9] C. Wang, D. Baer, L. Thomas, J. Amonette, J. Antony, Y. Qiang, G. Duscher, Void formation during early stages of passivation: Initial oxidation of iron nanoparticles at room temperature, J. Appl. Phys. 98 (2005).
[10] C. Wang, D. Baer, J. Amonette, M. Engelhard, J. Antony, Y. Qiang, Morphology and electronic structure of the oxide shell on the surface of iron nanoparticles, J. Am. Chem. Soc. 131 (2009) 8824–8832.
[11] Q. Wang, S. Lee, H. Choi, Aging study on the structure of Fe0-nanoparticles: stabilization, characterization, and reactivity, J. Phys. Chem. C. 114 (2010) 2027–2033.
[12] L. Greenlee, J. Torrey, R. Amaro, J. Shaw, Kinetics of zero valent iron nanoparticle oxidation in oxygenated water, Environ. Sci. Technol. 46 (2012) 12913–12920.
[13] V. Sarathy, P. Tratnyek, J. Nurmi, D. Baer, J. Amonette, C. Chun, R. Penn, E. Reardon, Aging of iron nanoparticles in aqueous solution: effects on structure and reactivity, J. Phys. Chem. C. 112 (2008) 2286–2293.
[14] X. Liu, F. Millero, The solubility of iron hydroxide in sodium chloride solutions, Geochim. Cosmochim. Acta 63 (1999) 3487–3497.
[15] U. Schwertmann, R. Cornell, Iron Oxides in the Laboratory: Preparation and Characterization, 2nd ed., Wiley, 2000.
[16] C. Noubactep, Processes of contaminant removal in Fe^0-H_2O systems revisited: The importance of co-precipitation, Open Environ. J. 1 (2007) 9–13.
[17] C. Noubactep, A critical review on the process of contaminant of contaminant removal in Fe^0–H_2O systems, Environ. Technol. 29 (2008) 909–920.
[18] A. Liu, J. Liu, B. Pan, W. Zhang, Formation of lepidocrocite (γ-FeOOH) from oxidation of nanoscale zero-valent iron (nZVI) in oxygenated water, RSC Adv. 4 (2014) 57377–57382.
[19] S. Kanel, B. Manning, L. Charlet, H. Choi, Removal of arsenic(III) from groundwater by nanoscale zero-valent iron, Environ. Sci. Technol. 39 (2005) 1291–1298.
[20] S. Ponder, J. Darab, T. Mallouk, Remediation of Cr(VI) and Pb(II) aqueous solutions using supported, nanoscale zero-valent iron, Environ. Sci. Technol. 34 (2000) 2564–2569.
[21] S. Morrison, D. Metzler, B. Dwyer, Removal of As, Mn, Mo, Se, U, V and Zn from groundwater by zero-valent iron in a passive treatment cell: reaction progress modeling, J. Contam. Hydrol. 56 (2002) 99–116.
[22] H. Kim, J. Ahn, K. Hwang, I. Kim, H. Inseong, Atmospherically stable nanoscale zero-valent iron particles formed under controlled air contact: Characteristics and reactivity, Environ. Sci. Technol. 44 (2010) 1760–1766.
[23] H. Kim, T. Kim, J. Ahn, K. Hwang, J. Park, T. Lim, I. Hwang, Aging characteristics and reactivity of two types of nanoscale zero-valent iron particles (FeBH and FeH_2) in nitrate reduction, Chem. Eng. J. 197 (2012) 16–23.
[24] B.C. Reinsch, B. Forsberg, R.L. Penn, C.S. Kim, G.V. Lowry, Chemical transformations during aging of zerovalent iron nanoparticles in the presence of common groundwater dissolved constituents, Environ. Sci. Technol. 44 (2010) 3455–3461.
[25] Y. Liu, S. Majetich, R. Tilton, D. Sholl, G. Lowry, TCE dechlorination rates, pathways, and efficiency of nanoscale iron particles with different properties, Environ. Sci. Technol. 39 (2005) 1338–1345.
[26] Y. Liu, H. Choi, D. Dionysiou, G. Lowry, Trichloroethene hydrodechlorination in water by highly disordered monometallic nanoiron, Chem. Mater. 17 (2005) 5315–5322.
[27] D. O'Carroll, B. Sleep, M. Krol, H. Boparai, C. Kocur, Nanoscale zero valent iron and bimetallic particles for contaminated site remediation, Adv. Water Resour. 51 (2013) 104–122.
[28] G. Glavee, K. Klabunde, C. Sorensen, G. Hadjipanayis, Chemistry of borohydride reduction of iron(II) and iron(III) ions in aqueous and nonaqueous media. Formation of nanoscale Fe, FeB, and Fe_2B Powders, Inorg. Chem. 34 (1995) 28–35.
[29] C. Wang, W. Zhang, Synthesizing nanoscale iron particles for rapid and complete dechlorination of TCE and PCBs, Environ. Sci. Technol. 31 (1997) 2154–2156.
[30] X. Li, W. Zhang, Sequestration of metal cations with zerovalent iron nanoparticles: a study with high resolution X-ray photoelectron spectroscopy (HR-XPS), J. Phys. Chem. 111 (2007) 6939–6946.
[31] N. Fairley, CasaXPS: Processing Software for XPS, AES, SIMS and more, 2005, <http://www.casaxps.com/> (accessed 27.05.15).
[32] A.P. Grosvenor, B.A. Kobe, M.C. Biesinger, N.S. McIntyre, Investigation of multiplet splitting of Fe 2p XPS spectra and bonding in iron compounds, Surf. Interface Anal. 36 (2004) 1564–1574.
[33] H. Abdel-Samad, P. Watson, An XPS study of the adsorption of chromate on goethite (α-FeOOH), Appl. Surf. Sci. 108 (1997) 371–377.
[34] B. Ravel, M. Newville, ATHENA and ARTEMIS interactive graphical data analysing using IFEFFIT, Phys. Scr. 2005 (2005) 1007–1010.
[35] L. Signorini, L. Pasquini, L. Savini, R. Carboni, F. Boscherini, E. Bonetti, A. Giglia, M. Pedio, N. Mahne, S. Nannarone, Size-dependent oxidation in iron/iron oxide core-shell nanoparticles, Phys. Rev. B. 68 (2003) 1–8.
[36] R. Cornell, U. Schwertmann, The iron oxides. Structure, Properties, Reactions, Occurrences and Uses, 2nd ed., Wiley, Darnstadt, 2003.
[37] Y. Sun, X. Li, J. Cao, W. Zhang, H. Wang, Characterization of zero-valent iron nanoparticles, Adv. Colloid Interface Sci. 120 (2006) 47–56.
[38] R. Johnson, J. Nurmi, G. O'Brien Johnson, D. Fan, R. O'Brien Johnson, Z. Shi, A. Salter-Blanc, P. Tratnyek, G. Lowry, Field-scale transport and transformation of carboxymethylcellulose-stabilized nano zero-valent iron, Environ. Sci. Technol. 47 (2013) 1573–1580.
[39] D. Baer, D. Gaspar, P. Nachimuthu, S. Techane, D. Castner, Application of surface chemical analysis tools for characterization of nanoparticles, Anal. Bioanal. Chem. 396 (2010) 983–1002.
[40] K. Siskova, J. Tucek, L. MacHala, E. Otyepkova, J. Filip, K. Safarova, J. Pechousek, R. Zboril, Air-stable nZVI formation mediated by glutamic acid: Solid-state storable material exhibiting 2D chain morphology and high reactivity in aqueous environment, J. Nanoparticle Res. 14 (2012) 1–13.
[41] A. Pratt, L. Lari, O. Hovorka, A. Shah, C. Woffinden, S. Tear, C. Binns, R. Kröger, Enhanced oxidation of nanoparticles through strain-mediated ionic transport, Nat. Mater. 13 (2014) 26–30.
[42] C. Noubactep, S. Caré, R. Crane, Nanoscale metallic iron for environmental remediation: prospects and limitations, Water Air Soil Pollut. 223 (2012) 1363–1382.
[43] R. Crane, H. Pullin, J. Macfarlane, M. Similon, I. Popescu, M. Anderson, V. Calen, T. Scott, Field application of nanoscale zero-valent iron particles for the remediation of uranium bearing mine water, J. Environ. Eng. 141 (2014).
[44] R. Crane, T. Scott, The removal of uranium onto carbon-supported nanoscale zero-valent iron particles, J. Nanoparticle Res. 16 (2014).
[45] F. Maillot, G. Morin, Y. Wang, D. Bonnin, P. Ildefonse, C. Chaneac, G. Calas, New insight into the structure of nanocrystalline ferrihydrite: EXAFS evidence for tetrahedrally coordinated iron(III), Geochim. Cosmochim. Acta 75 (2011) 2708–2720.
[46] R. Eggleton, R. Fitzpatrick, New data and a revised structural model for ferrihydrite, Clays Clay Miner. 36 (1988) 111–124.
[47] M. Nagayama, M. Cohen, The anodic oxidation of iron in a neutral solution, J. Electrochem. Soc. 109 (1962) 781–790.
[48] M. Morris, Octahedral vs. Tetrahedral: Crystal Field Theory, 2012, http://www.mjmorris.staff.shef.ac.uk/teaching/CHM1002/lect3b.html.
[49] N. McIntyre, D. Zetaruk, X-ray photoelectron spectroscopic studies of iron oxides, Anal. Chem. 49 (1977) 1521–1529.
[50] M. Sheydaei, S. Aber, Preparation of nano-lepidocrocite and an investigation of its ability to remove a metal complex dye, CLEAN – Soil, Air, Water 41 (2013) 890–898.
[51] H. Park, P. Ayala, M. Deshusses, A. Mulchandandi, H. Choi, N. Myung, Electrodeposition of maghemite (γ-Fe_2O_3) nanoparticles, Chem. Eng. J. 139 (2008) 208–212.
[52] H. Guo, A. Barnard, Naturally occurring iron oxide nanoparticles: morphology, surface chemistry and environmental stability, J. Mater. Chem. A. 1 (2013) 27–42.
[53] C. Su, R. Puls, T. Krug, M. Watling, S. O'Hara, J. Quinn, N. Ruiz, Travel distance and transformation of injected emulsified zerovalent iron nanoparticles in the subsurface during two and half years, Water Res. 47 (2013) 4095–4106.
[54] S. Fuller, D. Stewart, I. Burke, Chromate reduction in highly alkaline groundwater by zerovalent iron: implications for its use in a permeable reactive barrier, Ind. Eng. Chem. Res. 52 (2013) 4704–4714.

[55] X. Li, L. Lei, C. Yang, W. Zhang, Reduction of Cr(VI) by nanoscale zero valent iron (nZVI): The reaction kinetics, 2010 4th Int. Conf. Bioinforma. Biomed. Eng. iCBBE 2010. (2010) 1–4.
[56] S. Fendorf, G. Li, Kinetics of chromate reduction by ferrous iron, Environ. Sci. Technol. 30 (1996) 1614–1617.
[57] L. Eary, D. Rai, Chromate removal from aqueous wastes by reduction with ferrous iron, Environ. Sci. Technol. 22 (1988) 972–977.
[58] C. Hu, S. Lo, Y. Liou, Y. Hsu, K. Shih, C. Lin, Hexavalent chromium removal from near natural water by copper-iron bimetallic particles, Water Res. 44 (2010), 3101-3018.
[59] S. Chowdhury, E. Yanful, A. Pratt, Chemical states in XPS and Raman analysis during removal of Cr(VI) from contaminated water by mixed maghemite-magnetite nanoparticles, J. Hazard. Mater. 235–236 (2012) 246–256.
[60] Q. Wang, H. Qian, Y. Yang, Z. Zhang, C. Naman, X. Xu, Reduction of hexavalent chromium by carboxymethyl cellulose-stabilized zero-valent iron nanoparticles, J. Contam. Hydrol. 114 (2010) 35–42.
[61] S. Ponder, J. Darab, J. Bucher, D. Caulder, I. Craig, L. Davis, N. Edelstein, W. Lukens, H. Nitsche, L. Rao, D. Shuh, T. Mallouk, Surface chemistry and electrochemistry of supported zerovalent iron nanoparticles in the remediation of aqueous metal contaminants, Chem. Mater. 13 (2001) 479–486.
[62] X. Li, J. Cao, W. Zhang, Stoichiometry of Cr(VI) immobilization using nanoscale zerovalent iron (nZVI): a study with high-resolution X-ray photoelectron spectroscopy (HR-XPS), Ind. Eng. Chem. Res. 47 (2008) 2131–2139.
[63] K. Sohn, S. Kang, S. Ahn, M. Woo, S. Yang, Fe(0) nanoparticles for nitrate reduction: stability, reactivity, and transformation, Environ. Sci. Technol. 40 (2006) 5514–5519.
[64] K. Ollila, Copper corrosion experiments under anoxic conditions, 2013, http://www.iaea.org/inis/collection/NCLCollectionStore/_Public/44/098/44098716.pdf (accessed 18.02.16).
[65] W. Yan, A. Herzing, C. Kiely, W. Zhang, Nanoscale zero-valent iron (nZVI): Aspects of the core-shell structure and reactions with inorganic species in water, J. Contam. Hydrol. 118 (2010) 96–104.